T.-T. Yen, A. P. Pisano, and C. T.-C. Nguyen, "High-*Q* capacitive-piezoelectric AlN lamb wave resonators," *Tech. Digest*, 2012 IEEE Int. Micro Electro Mechanical Systems Conference, Taipei, Taiwan, Jan. 20-24, 2013, pp. 114-117.

HIGH-*Q* CAPACITIVE-PIEZOELECTRIC ALN LAMB WAVE RESONATORS

T.-T. Yen[1], A. P. Pisano[1], and C. T.-C. Nguyen[1]
[1]Berkeley Sensor and Actuator Center, University of California at Berkeley, CA, USA

ABSTRACT

The use of capacitive-piezoelectric transducers, formed by separating a piezoelectric structure from its electrodes by sub-micron gaps, has raised the measured quality factor of aluminum nitride (AlN) Lamb wave resonators (LWR) from the ~1,000 of typical square-edged conventional devices (with contacting electrodes) to over 5,000 at 940 MHz, posting the highest reported Q for non-overmoded pure AlN resonators using d_{31} (e_{31}) transduction at this frequency range. The $Q \cdot f$ product achieved here is significantly higher than that of a previous 1.2-GHz capacitive-piezoelectric contour-mode ring, mainly due to the use of Lamb wave modes that allow better support isolation to prevent energy loss to the substrate. In addition, the use of interdigital transducer (IDT) electrodes successfully decouples the resonance frequency from overall device dimensions, offering a CAD-definable design parameter for fine-frequency control. The effective coupling coefficient of $k_{eff}^2 = 0.3\%$ achieved by this device is lower than the 1.6% typically observed for conventional AlN Lamb wave resonators, but still sufficient to avoid pass-band distortion in the 0.1% bandwidth filters needed for next-generation RF channel-selecting communication front-ends.

INTRODUCTION

Given that the insertion loss of any bandpass filter is proportional to $\omega_o/(Q \cdot B)$—where ω_o is its radian center frequency, B its bandwidth, and Q the quality factor of its constituent resonators—high resonator Q is especially important for small percent bandwidth filters. In recent years, this fact has driven efforts to maximize resonator Q for use in advanced RF channel-select communication schemes that utilize a bank of narrowband filters to eliminate not only out-of-band blockers, but also in-band ones, thereby allowing use of a receiver architecture with substantially reduced power consumption [1]. Among available resonators, capacitive-gap transduced ones constructed in poly-Si or diamond easily achieve the Q's greater than 20,000 needed for RF channel-selection at GHz frequencies [2], but suffer from high motional impedance. In the meantime, resonators using piezoelectric transduction [3] offer low motional impedance but insufficient Q (~1,500) for RF channel-selection.

According to energy loss theory [4, 5], silicon's $Q \cdot f$ product ceiling due to phonon-phonon interaction should only be about 3 to 3.5 times larger than that of AlN. Interestingly, the measured quality factors of conventional AlN resonators are generally one to two orders smaller than that of capacitive-gap transduced poly-Si resonators at similar frequencies. This observation implies that modern piezoelectric devices are still plagued by non-intrinsic loss mechanisms (*e.g.*, due to electrodes, anchors, *etc.*). Indeed, instead of AlN material properties and device geometries, metal electrode damping and interface strain might be the real culprits responsible for the Q limits of conventional piezoelectric resonators.

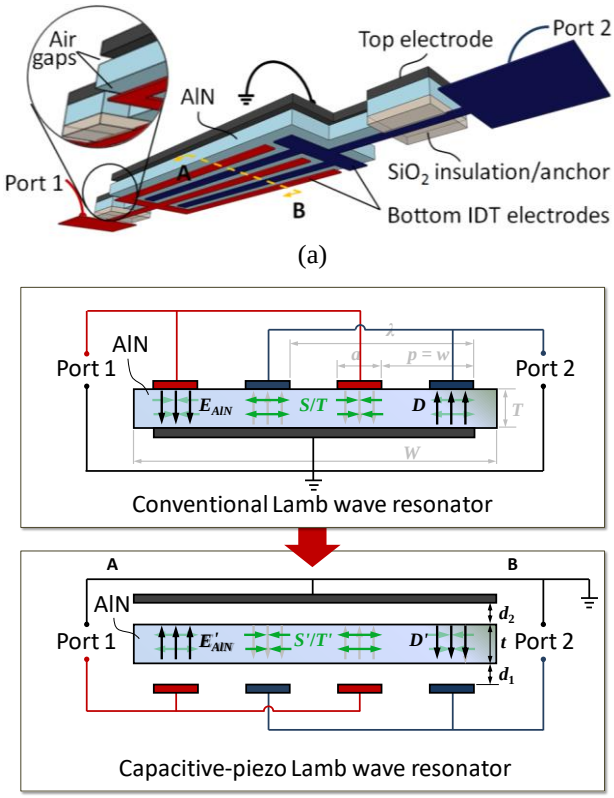

Figure 1: (a) Perspective-view illustration of a capacitive-piezo Lamb wave resonator and (b) its cross-section alongside that of a conventional device with contacting electrodes. The capacitive-piezo AlN resonator structure is separated from its top and bottom electrodes by distances d_1 and d_2, respectively.

Capacitive-Piezoelectric Transduction

Benson first postulated that this might be true as far back as the 1970s, when he suggested that the main constraint on the Q's of high frequency conventional quartz resonators arises from metallic electrode deposition [6, 7]. In fact, numerous experimental data at the time showed that both Q and resonance frequency decrease with increasing metal electrode thickness [8]. These observations eventually led to the demonstration of the *spaced-electrode* quartz BVA resonator design, which used a non-contacting electrode to alleviate or eliminate such electrode-derived problems as damping, stress, contamination, and ion migration. With this design, quartz resonators at frequencies of a few megahertz with quality factors approaching the material limit were soon reported [6, 7].

More recently, Hung *et al.* applied this approach to MEMS-based piezoelectric AlN ring and disk resonators and demonstrated some of the highest Q's yet seen in AlN resonators, with values >12,000 in the 50 MHz range [9] and >3,000 at 1.2 GHz [10], all while simultaneously maintaining decent motional resistance under 1 kΩ. Although impressive, these results are still not sufficient for

RF channel-selection, where GHz quality factors above 20,000 are generally required.

Capacitive-Piezoelectric Lamb Wave Resonator

Pursuant to improving upon this, Figure 1 presents a perspective-view illustration and cross-section of the capacitive-piezoelectric AlN Lamb wave resonator demonstrated via this work. As in the work of [9], to minimize damping and interface strain caused by metal electrodes, the Lamb wave resonators demonstrated here use *piezoelectric* AlN as the resonator structure, but incorporate *capacitive electrode-to-resonator gaps* to couple in electric fields, thereby effectively realizing a combined "*capacitive-piezo*" transducer. The introduction of air gaps between the piezoelectric resonator structure and its metal electrodes eliminates metal-to-AlN interface losses and metal damping to enable high Q; while the sub-micron spacings of the gaps still allow strong electric fields across the piezoelectric resonator, preserving high electromechanical coupling and adequate motional impedance.

To operate this device, an AC voltage applied across the input electrodes generates an electric field E_{AlN}' across the piezoelectric layer that induces mechanical stress and strain (T' and S') via the reverse-piezoelectric effect. When the input AC signal matches the resonance frequency of the device, an acoustic vibration with half-wavelength equaling the IDT electrode pitch p is excited, generating a Lamb wave propagating through the AlN plate. At the output electrode, by means of the direct-piezoelectric effect, the mechanical stress and strain caused by Lamb wave mode vibration induce an electrical displacement current D' that generates opposite AC charges on opposing AlN surfaces, which are then collected by the output electrodes to deliver an output signal proportional to the displacement.

DEVICE MODELING

Figure 2 presents a cross-section of the capacitive-piezo Lamb wave resonator overlaid by its equivalent electrical circuit. Here, the air gaps are modeled as two capacitors, C_{g1} and C_{g2}, in series with the piezoelectric structure, itself modeled by static capacitor C_0. When a sinusoidal input voltage V_{in} is applied across the top and bottom electrodes, mechanical strain is induced in the AlN film. However, if the air gaps are taken into account, the effective electric field across the AlN film, E_{AlN}', degrades by a correction factor κ, and can be expressed as

$$E_{AlN}' = \frac{V_{in}}{t + \varepsilon_r d} = \frac{V_{in}}{t} \cdot \kappa = E_{AlN} \cdot \kappa \tag{1}$$

where $d = d_1 + d_2$ is the total gap spacing, ε_r is the c-axis relative permittivity of AlN, and E_{AlN} is the electric field across the AlN film in the conventional case (*i.e.*, $d = 0$). From (1), the correction factor κ takes the form

$$\kappa = \frac{t}{t + \varepsilon_r d} \leq 1 \tag{2}$$

Expressions for important resonator metrics (*e.g.*, k_{eff}^2) are perhaps best obtained via an equivalent circuit modeling a single port with all others grounded, such as depicted in Figure 3(a). Here, the impedance of the single port is now modeled as a classic BVD circuit in series with the effective capacitor C_g contributed by the two air gap capacitors of Figure 2, where $C_g = C_{g1} \cdot C_{g2} / (C_{g1} + C_{g2})$. It is convenient to further absorb the C_g into the BVD circuit to

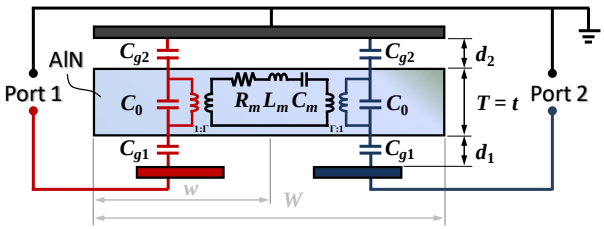

Figure 2: Equivalent circuit overlaid atop a capacitive-piezo Lamb wave resonator schematic, where the air gap capacitors are modeled by C_{g1} and C_{g2}. Alternating IDT bottom electrodes connect to the input and output ports, respectively.

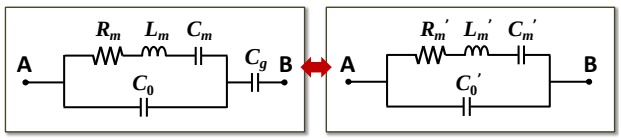

(a) (b)

Figure 3: (a) Equivalent BVD model of a one-port resonator in series with an air-gap capacitor C_g, and (b) alternative form of the same circuit obtained by absorbing the air-gap capacitor into a classic BVD topology.

yield the circuit of Figure 3(b) with new lumped element values given by

$$R_m' = \left(\frac{C_g + C_0}{C_g} \right)^2 \cdot R_m \tag{3}$$

$$L_m' = \left(\frac{C_g + C_0}{C_g} \right)^2 \cdot L_m \tag{4}$$

$$C_m' = \frac{C_g^2 \cdot C_m}{(C_g + C_0)(C_m + C_g + C_0)} \approx \left(\frac{C_g}{C_g + C_0} \right)^2 \cdot C_m \tag{5}$$

$$C_0' = \frac{C_g}{C_g + C_0} \cdot C_0 \tag{6}$$

Using (5) and (6), the static-to-motional capacitance ratio then takes the form

$$C_r' = \frac{C_0'}{C_m'} = \frac{C_m + C_g + C_0}{C_g} \cdot \frac{C_0}{C_m} \approx \frac{C_g + C_0}{C_g} \cdot C_r \tag{7}$$

The common factor $C_g/(C_g+C_0)$ permeates all of Equations (3) to (7), where the motional elements of a capacitive-piezo resonator scale relative to those of a conventional piezoelectric resonator by the square of this term, and the static capacitance depends linearly on the same term. Not surprisingly, this ratio can be shown to equal the correction factor κ already defined in Equation (8):

$$\frac{C_g}{C_g + C_0} = \frac{\frac{\varepsilon_0 A}{d}}{\frac{\varepsilon_0 A}{d} + \frac{\varepsilon_0 \varepsilon_r A}{t}} = \frac{t}{t + \varepsilon_r d} = \kappa \leq 1 \tag{8}$$

Note that above approximations are valid for the typical case when $C_m << C_0 < C_g$.

To gauge the impact of the electrode-to-resonator gaps on electromechanical coupling, use of the above equations yields for the series and parallel resonance frequencies of the capacitive-piezo resonator:

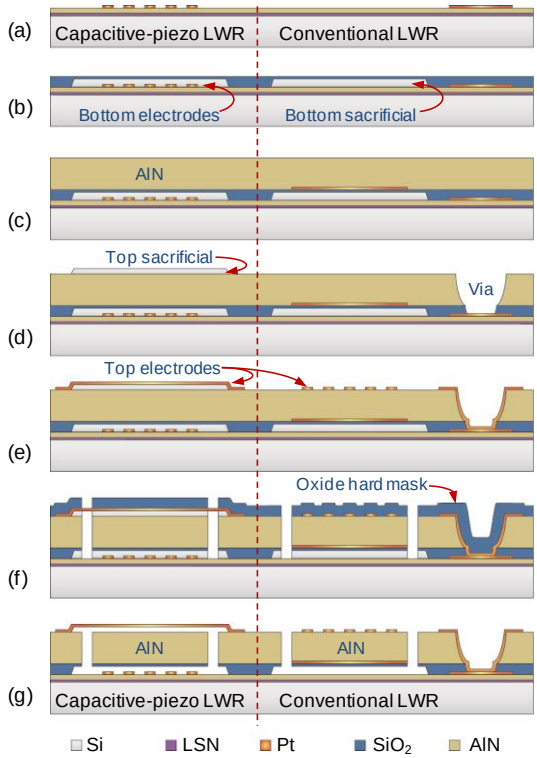

Figure 4: Fabrication process for co-fabrication of conventional and capacitve-piezo Lamb wave devices.

$$f_s' = \frac{1}{2\pi}\sqrt{\frac{1}{L_m' C_m'}} = \sqrt{1+\frac{C_m}{C_g + C_0}} \cdot f_s \approx f_s \qquad (9)$$

$$f_p' = \sqrt{1+\frac{C_m'}{C_0'}} \cdot f_s' \approx \sqrt{1+\kappa \cdot \frac{C_m}{C_0}} \cdot f_s' \qquad (10)$$

Equation (10) indicates that the addition of electrode-to-resonator gaps reduces somewhat the parallel resonance frequency in a similar fashion to the way connecting a variable capacitor in series with a mechanical resonator offers a method to fine tune the parallel resonance frequency at the expense of increased C_r. On the other hand, the series resonance frequency remains unchanged. This means f_s' and f_p' are now closer together in the inductive region, which indicates a reduced coupling coefficient. The effective coupling coefficient for this capacitive-piezo resonator now takes the form

$$k_{eff}^2{}' \approx \frac{\pi^2}{4} \cdot \frac{f_p' - f_s'}{f_p'} \approx \frac{\pi^2}{8} \cdot \frac{C_m'}{C_0'} \approx \kappa \cdot k_{eff}^2 \qquad (11)$$

where k_{eff}^2 is the effective coupling coefficient of a conventional electrode-loaded Lamb wave resonator. Again, $k_{eff}^2{}'$ is smaller than its conventional counterpart by the correction factor κ. To avoid excessive reduction in coupling, the gap spacing should be chosen small enough so that $C_m << C_0 < C_g$.

DEVICE FABRICATION

Figure 4 presents the fabrication process flow used in this work, which features a buried sacrificial layer that facilitates co-fabrication of both conventional and capacitive-piezo Lamb wave resonators on the same wafer to facilitate a fair comparison.

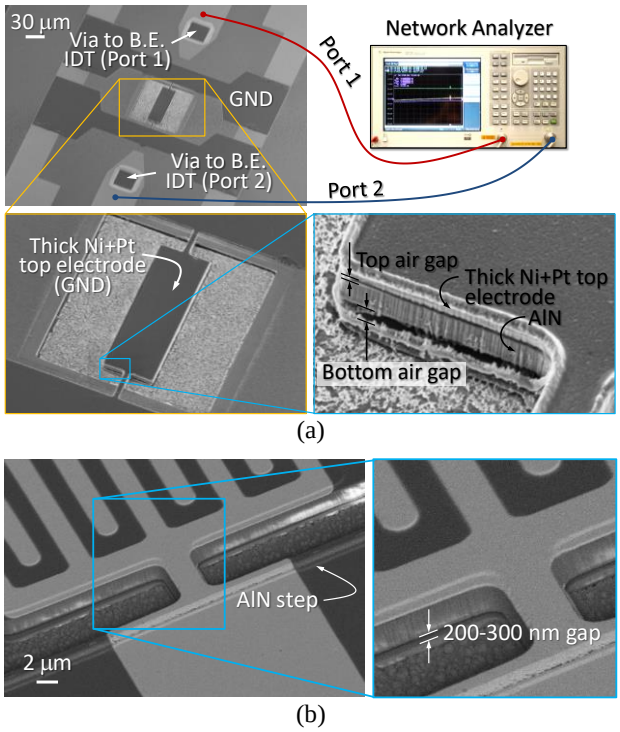

Figure 5: SEM images of (a) a capacitive-piezo Lamb wave resonator and (b) a conventional device fabricated in the same process flow.

The fabrication process starts with sequential depositions of thin low-stress nitride (LSN) and AlN insulating films over a high resistivity silicon substrate. A Chromium/Platinum (Cr/Pt) bottom electrode layer is then deposited on a patterned dual-layer (G-line and I-line) photoresist characterized to achieve clean and smooth edges after a lift-off process (*cf.* Figure 4(a)). Next, patterned IDT bottom electrodes are buried under a blanket-deposited poly-Si bottom sacrificial layer, which is then chemical-mechanical polished (CMP'ed) to flatten its surface, *i.e.*, reduce its surface topography. This CMP step also sets the electrode-to-resonator gap distance d_1, which means it also determines the value of C_{g1} and influences the resonance frequency and the coupling coefficient of the eventual resonator device. Low temperature oxide (LTO) is then deposited to bury the bottom poly-Si sacrificial layer, followed by a critical CMP process (*cf.* Figure 4(b)) to provide a smooth surface for AlN growth. This LTO layer can also serve as passive thermal compensation.

Once a flat substrate is obtained, a Cr/Pt middle electrode layer (the bottom electrode for conventional Lamb wave resonators) is deposited and patterned, followed by sputter deposition of 1.5 µm-thick AlN resonator structural material (*cf.* Figure 4(c)). The preceding planarization step is key to achieving a highly oriented AlN thin film with a full-width-half-magnitude (FWHM) value of 1.4°.

Next, an amorphous-silicon (a-Si) top sacrificial layer is deposited and patterned to keep electrode-to-resonator spacings above capacitive-piezo devices, but remove them above conventional devices. Vias are then etched into the AlN layer to reach bottom electrodes where needed (*cf.* Figure 4(d)). The top Cr/Pt electrode is then deposited and patterned, followed by electroplating of a thick low stress nickel (Ni) layer over the top electrodes for structural

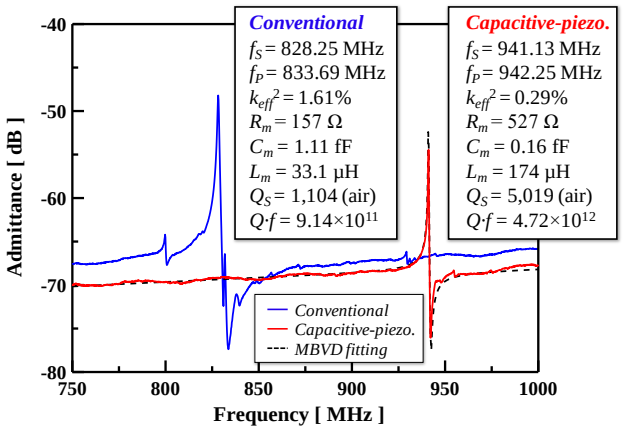

Figure 6: Measured admittance plots for one-port capacitive-piezo and conventional Lamb wave resonators.

support and to reduce electrode parasitic resistance. Figure 4(e) shows the cross-section view after these steps.

To define the resonator geometry, a PECVD SiO_2 layer is first deposited and patterned to serve as a hard mask, through which a BCl_3-based RIE defines AlN Lamb wave resonators and tethers. After etching through AlN, a CF_4-based RIE is used to remove remaining oxide hard mask in places, while simultaneously defining the thermal compensation oxide layer (*cf.* Figure 4(f)). The wafer is then diced and released using a dry isotropic XeF_2 etch (*cf.* Figure 4(g)). Figure 5 presents SEM images of a released capacitive-piezoelectric Lamb wave resonator with sub-micron electrode-to-resonator gaps; and a conventional device fabricated in the same process flow.

MEASUREMENT & DISCUSSION

Figure 6 presents one-port admittance response spectra measured in air for a capacitive-piezo and a conventional Lamb wave resonator fabricated on the same substrate. The air gaps enable a measured quality factor for the capacitive-piezo Lamb wave resonator over 5,000 at 940 MHz and a $Q \cdot f$ product above 4.7×10^{12} that now sets the mark for non-overmoded pure AlN resonators using d_{31} (e_{31}) transduction at this frequency range [11].

The use of interdigital transducer (IDT) electrodes successfully decouples the resonance frequency from overall device dimensions, offering a CAD-definable design parameter for fine-frequency control. Although the two devices were designed to have the same IDT electrode pitch, a significant frequency shift is observed, mainly due to the elimination of electrode mass loading. This should not be confused with frequency shifts predicted by Equations (9) and (10).

Compared with conventional Lamb wave resonators with contacting electrodes, the coupling coefficient of these spaced-electrode devices do inevitably decrease from above 1.6% to 0.3%. However, this value is still sufficient to attain the 0.1%-bandwidth filters required for RF channel-selection without pass-band distortion. Likewise, although the motional impedances of these devices do rise from 150 Ω to 500 Ω, this value is still much lower than so far achieved by capacitive-gap transduced devices at this frequency and can be easily terminated via on-chip matching networks, or even directly matched to on-chip transistor electronics.

CONCLUSIONS

By merely introducing sub-micron gaps between a Lamb wave AlN resonator and its electrodes, the capacitive-piezo transducers of this work enable a measured quality factor over 5,000 at 940 MHz and a $Q \cdot f$ product above 4.7×10^{12} that now sets the mark for non-overmoded pure AlN resonators using d_{31} (e_{31}) transduction at this frequency range and brings AlN technology ever closer to the Q bogy needed for next-generation RF channel-selecting communication front-ends. However, these Q benefits are accompanied by an increased capacitance ratio C_r and by changes in device characteristics, including its parallel resonance frequency and coupling coefficient. In particular, the electromechanical coupling of $k_{eff}^2 = 0.3\%$ achieved by this device is lower than the 1.6% typically observed for conventional AlN Lamb wave resonators, but still sufficient to avoid pass-band distortion in the 0.1% bandwidth filters needed for RF channel-selection. If higher coupling is desired, the electrode-to-resonator gaps must be made smaller, on the order of less than 100 nm—something already achieved in capacitive-gap transduced resonators, so probably reasonable for future capacitive-piezo ones.

ACKNOWLEDGEMENTS

The authors would like to offer special thanks to the staff of the Berkeley Marvell Nanofabrication Laboratory, especially Xiaofan Meng, Joe Donnelly, and Jay Morford, for their invaluable assistance.

REFERENCES

[1] C. T. C. Nguyen, "Frequency-selective MEMS for miniaturized low-power communication devices," *Microwave Theory and Techniques, IEEE Transactions on*, vol. 47, pp. 1486-1503, 1999.

[2] T. L. Naing *et al.*, "2.97-GHz CVD diamond ring resonator with Q > 40,000," in *IEEE FCS'12*, pp. 1-6.

[3] G. Piazza *et al.*, "Piezoelectric aluminum nitride vibrating contour-mode MEMS resonators," *JMEMS*, vol. 15, pp. 1406-1418, 2006.

[4] V. B. Braginsky *et al.*, *Systems with Small Dissipation*: University of Chicago Press, 1985.

[5] S. A. Chandorkar *et al.*, "Limits of quality factor in bulk-mode micromechanical resonators," *MEMS'08, pp. 74-77*.

[6] R. J. Besson, "A new "electrodeless" resonator design," *31st Annual Frequency Control Symposium*, pp. 147-152, 1977.

[7] R. J. Besson *et al.*, "Further advances on B.V.A. quartz resonators," *34th Annual Frequency Control Symposium*, pp. 175-182, 1980.

[8] C. G. Courcimault *et al.*, "High-Q mechanical tuning of MEMS resonators using a metal deposition-annealing technique," *TRANSDUCERS '05*, pp. 875-878.

[9] L.-W. Hung *et al.*, "Capacitive-piezoelectric AlN resonators with Q>12,000," *MEMS'11*, pp.173-176.

[10] L.-W. Hung *et al.*, "Capacitive-piezo transducers for higher Q contour-mode AlN resonators at 1.2GHz," *Hilton Head'10*, pp. 463-466.

[11] R. Ruby *et al.*, "Method of extracting unloaded Q applied across different resonator technologies," *IEEE IUS'08*, pp. 1815-1818.

CONTACT

*T.-T. Yen, tel: +1-510-3870301; ernest.ttyen@gmail.com